

Impact of precession on the climate, vegetation and fire activity in southern Africa during MIS4

M.-N. Woillez^{1,2,3}, G. Levvasseur⁴, A.-L. Daniau¹, M. Kageyama⁵, D.H. Urrego^{1,2,3}, M.-F. Sánchez-Goñi², and V. Hanquiez¹

¹Centre National de la Recherche Scientifique (CNRS), Environnements et Paléocénvironnements Océaniques et Continentaux (EPOC), Unité Mixte de Recherche (UMR) 5805, Université Bordeaux 1, F-33400 Talence, France

²Ecole Pratique des Hautes Etudes (EPHE), EPOC, UMR 5805, F-33400 Talence, France

³CNRS, de la Préhistoire à l'Actuel: Culture, Environnement et Anthropologie (PACEA), UMR 5199, F-33400 Talence, France

⁴Institut Pierre Simon Laplace, Pôle de Modélisation du Climat, Université Pierre et Marie Curie, 4 Place Jussieu, Paris.

⁵LSCE/IPSL INSU, UMR 8212, CE Saclay, l'Orme des Merisiers, 91191 Gif-sur-Yvette Cedex, France

Correspondence to: M.-N. Woillez
(marienoelle.woillez@gmail.com)

Abstract.

The relationships between climate, vegetation and fires are a major subject of investigation in the context of climate change. In southern Africa, fire is known to play a crucial role in the existence of grasslands and Mediterranean-type biomes. Microcharcoal-based reconstructions of past fire activity in that region have shown a tight correlation between grass-fueled fires and the precessional cycle, with maximum fire activity during maxima of the climatic precession index. These changes have been interpreted as the result of changes in fuel load in response to precipitation changes in eastern southern Africa. Here we use the general circulation model IPSL_CM5A and the dynamic vegetation model LPJ-LMfire to investigate the response of climate, vegetation and fire activity to precession changes in southern Africa during Marine Isotopic Stage 4 (74-59 kyr BP). We perform two climatic simulations, for a maximum and minimum of the precession index, and use a statistical downscaling method to increase the spatial resolution of the IPSL_CM5A outputs over southern Africa and perform high-resolution simulations of the vegetation and fire activity. Our results show an anti-correlation between the North and South African monsoons in response to precession changes. A decrease of the precession climatic index leads to a precipitation decrease in the summer rainfall area of southern Africa. The drying of climate leads to a decrease of vegetation cover and fire activity. Our results are in qualitative agreement with data and confirm that fire activity in southern Africa during MIS4 is mainly driven by vegetation cover.

1 Introduction

The relationships between climate, ecosystems and fire are currently a major concern in the context of future climate change, as fire risk is expected to increase in several regions worldwide in response to both the rise in temperature and precipitation decrease (Liu *et al.*, 2010). However the studies on this issue are usually based on predicted temperature and precipitation changes only (Liu *et al.*, 2010). They do not take into account possible shifts in the ecosystems, which would change the amount of fuel available or its composition, such as the ratio from coarse fuels to fine fuels and the flammability of fuel components, which in turn will affect fire intensity and frequency (e.g. Daniau *et al.* (2007)). This is particularly true for southern Africa, a land of contrasted climates and ecosystems. The western part receives less than 250 mm/year of precipitation and is occupied by desert and semi-desert biomes (Cowling *et al.*, 1997). The eastern part is under the remote influence of the Intertropical Convergence Zone (ITCZ) and precipitation occurs during austral summer (November-March), when the ITCZ is at its southernmost position. In that region, annual precipitation amounts range from 500 mm/year to more than 1250 mm/year and allow the development of forests and savanna along the coast and grasslands in the more central regions (Cowling *et al.*, 1997). The Cape region receives precipitation during the austral winter and the landscape is dominated by *Fynbos*, a Mediterranean-type biome composed of evergreen shrubs. No fires occur in the desert and semi-desert regions due to the scarcity of fuel load, but the eastern grasslands and the southwestern *Fynbos* are under the influence of an important fire activity, occurring mainly during the dry season, i.e. during austral winter and austral summer respectively (Archibald *et al.*, 2010). Fire exclusion experiments performed in southern Africa suggest that fires play a crucial role in the existence of the grasslands and *Fynbos* and that without fires, climatic conditions would allow the development of forests in these regions (Westfall *et al.*, 1983; Titshall *et al.*, 2000). Simulations performed by Bond *et al.* (2003a,b) with a dynamic vegetation model including a fire module are consistent with these field experiments. In their simulations, forests cover the eastern part of southern Africa if fire disturbance is not taken into account.

Daniau *et al.* (2013) have analyzed microcharcoal concentrations in a marine sediment core off southwestern Africa and interpreted this marker as a record of past fire activity. The record, which covers the period from 170 kyr BP to 30 kyr BP, exhibits a tight correlation between grass-fueled fires and the precessional cycle, with maximum fire activity occurring during maxima of the climatic precession index ($e \sin \omega$, with e the eccentricity and ω the longitude of the perihelion), when the boreal winter solstice occurs near the perihelion. Daniau *et al.* (2013) hypothesized that the variations in fire activity reflect precipitation changes in the grassy regions of eastern southern Africa, i.e. in the summer rainfall area. The decrease in solar radiation during austral summer associated with a low precession index would weaken the ITCZ convection and bring less rainfall over southern Africa. A drier austral summer would lead to a decrease in the biomass of grassy vegetation, less fuel would be available during the dry season and fire activity would decrease. This study presents

two interesting results: first, it suggests that in southern Africa a drier summer climate leads to a decrease rather than an increase in fire activity. Secondly it supports the link between precession and precipitation changes in southern Africa suggested by Partridge *et al.* (1997) and Kristen *et al.* (2007), based on lacustrine sediments analysis from northeastern Southern Africa.

60 Similarly, different paleoclimatic records (e.g. Gasse (2000); Wang *et al.* (2005)) have shown the dominant role of precession in variations of the North African and Indian monsoons during the Pleistocene, with increasing precipitation amounts for low values of the precession index (boreal winter solstice near the aphelion). The main forcing is the increase of summer insolation in the northern hemisphere during precession index minima, leading to warmer temperatures and lower
65 pressures over the land masses and driving a more intense monsoonal flow. This interpretation has been confirmed by many numerical models for the Holocene (e.g. Braconnot *et al.* (2000); Braconnot & Marti (2003); Ohgaito & Abe-Ouchi (2007); Marzin & Braconnot (2009b,a)) and appears to remain a valid hypothesis even under glacial condition (Masson *et al.*, 2000). By contrast, only few empirical data on past environmental changes from the southern hemisphere are available and
70 palaeoclimatic records from southern Africa are particularly rare. Data from Partridge *et al.* (1997), Kristen *et al.* (2007), Daniau *et al.* (2013) suggest an anti-correlation between the southern African monsoon and the North African monsoon. To our knowledge no modeling study has yet been undertaken to investigate this hypothesis, neither has the link between precipitation, biomass burning and precession in southern Africa, in particular during glacial times, when the presence of northern
75 hemisphere ice sheets and lower levels of greenhouse gases might have changed the sensitivity of the monsoons to precession changes.

Southern Africa is also a place of special interest regarding human evolution: the oldest symbolic designs, indicating the emergence of modern human behavior, date to Marine Isotope Stage 4 (MIS4, ~74-59 kyr BP) (Jacobs *et al.*, 2008; Henshilwood *et al.*, 2002, 2009; d'Errico & Henshilwood, 2007). Reconstructing climate, vegetation and fire activity evolution in southern Africa,
80 through the study of marine and terrestrial archives or paleoclimatic simulations, is therefore an important task to address the aforementioned climatic, ecological and archeological questions.

Here we investigate the role of precession changes on the southern African climate, vegetation
85 and fire activity during MIS4 through numerical modeling. We use the Atmosphere-Ocean General Circulation Model (AOGCM) IPSL_CM5A (Dufresne *et al.*, 2013) to perform simulations at the beginning and end of MIS4, which correspond to a maximum and minimum of the precession index respectively. Vegetation and fire changes during these two periods are investigated with the dynamic vegetation model LPJ-LMfire (Pfeiffer *et al.*, 2013). Fire occurrence depends on environmental conditions at local scale (moisture, vegetation type, fuel amount and type). Using the relatively coarse
90 outputs from the GCM to force LPJ-LMfire would lead to unrealistic simulations of burnt areas. Therefore we use a statistical downscaling method to increase the spatial resolution of the GCM

outputs. The high resolution climatic fields we obtain are used to force LPJ-LMfire and simulate fire activity at local scale.

95 2 Methods

2.1 Climate model and boundary conditions

We use the IPSL (Institut Pierre-Simon Laplace) AOGCM in its version IPSL_CM5A (Dufresne *et al.*, 2013). The atmosphere is simulated with the LMDZ model (Hourdin *et al.*, 2006), coupled to the ocean model OPA8/NEMO (Madec *et al.*, 1998), through the OASIS coupler (Valcke, 2006).
100 The atmosphere is simulated on a regular grid with 96×95 grid pixels in *longitude* \times *latitude* at the global scale (i.e. a spatial resolution of about $3.75^\circ \times 1.9^\circ$) and 39 altitude levels, which allows the simulation of the stratosphere dynamics. The global ocean is simulated on an irregular horizontal grid of 182×142 points and 31 depth levels. Sea-ice is dynamically simulated with the LIM2 model (Fichefet & Morales-Maqueda, 1997, 1999). The land-surface types and resulting
105 atmosphere-surface exchanges are described by the ORCHIDEE model (Krinner *et al.*, 2005), at the same spatial resolution as for the atmosphere. In this version of IPSL_CM5A the vegetation is fixed according to its present-day distribution, including agriculture, but phenology is interactively computed, depending on the climatic conditions. The performances of this new version of the IPSL model for past climates (Mid-Holocene and Last Glacial Maximum) have been described in
110 Kageyama *et al.* (2013a,b).

We perform two simulations of the MIS4 climate, at 72 kyr and 60 kyr BP, corresponding to a maximum and minimum of the precession index respectively and hereafter labelled MIS4_max and MIS4_min. The boundary conditions are set as follows: for both simulations we use the ICE-
115 6G_Interim ice-sheet reconstructions (Argus & Peltier, 2010) for 16 kyr BP (unpublished data) as an analogue for the MIS4 ice sheets, as both periods exhibit approximately the same sea-level change (about 70 m lower than present-day, Waelbroeck *et al.* (2002)). The land-sea distribution and topography are modified accordingly to this lower sea-level. The greenhouse gas concentrations are fixed according to the ice-core records (Petit *et al.*, 1999; Spahni *et al.*, 2005) for 72 kyr and 60 kyr BP
120 (see Tab.1) and the orbital parameters are taken from Laskar *et al.* (2004) (Tab.1 and Fig.S1 in the Supplement).

The orbital configuration for MIS4_max is relatively close to present-day, with the boreal winter solstice near the perihelion. The configuration is opposite in MIS4_min, with the boreal winter
125 solstice occurring when the Earth is close to the aphelion (Fig.S1 in the Supplement). In the northern hemisphere, the precession decrease between the beginning (MIS4_max) and end (MIS4_min) of MIS4 correspond to an increase in solar radiation during boreal summer, with a maximum in July

(Fig.1) and to a decrease during boreal winter. In the southern hemisphere a positive anomaly occurs during late austral winter and spring (from July to November), with a maximum anomaly in October South of 60°S (Fig.1).

Both simulations are run about 600 years, until the surface climatic variables are at equilibrium, and we analyze averages over the last 60 years of each simulation.

2.2 The vegetation and fire model LPJ-LMfire

2.2.1 Model description

To simulate the vegetation and fire activity in southern Africa, we use the process-based dynamic global vegetation model (DGVM) LPJ-LMfire (Pfeiffer *et al.*, 2013), a new version of the LPJ model (Sitch *et al.*, 2003) which includes an improved version of the SPITFIRE fire module (Thonicke *et al.*, 2010). The model dynamically simulates 9 different plant functional types (PFTs) (7 woody PFTs, C3 and C4 grasses), as well as the productivity and the terrestrial carbon cycle, in response to the climatic forcings, insolation, atmospheric CO₂ level and competitiveness between the PFTs. The vegetation cover is described in fractions of grid-cell covered by the different PFTs, which can coexist on the same grid-cell. The fractional coverage of a given PFT depends on both the productivity and the individual density, which vary independently. The spatial resolution is the same as the climatic forcings chosen by user, 0.16° in our case (see section 2.2.2) and agricultural land use is not taken into account.

The vegetation simulated by the DGVM provides information about the fuel type and fuel load to the fire module. The fire module in turn computes fire occurrence, spread and impact on vegetation, depending on fuel information, meteorological conditions and ignition sources. Lightening strikes are the only source of ignition taken into account in our simulations.

We run LPJ-LMfire off-line, i.e. there is no vegetation feedback on climate. To drive the model we need information on climate, soils, topography and atmospheric CO₂ concentrations. The required climatic variables are monthly means of air temperature, the range of the diurnal cycle, precipitation, the number of wet days, cloudiness, wind speed and lightening strike frequency, with interannual variability. A weather generator implemented in the model produces daily values from the monthly data.

2.2.2 Forcing fields

To perform vegetation and fire simulations at high resolution, we use the IPSL_CM5A outputs down-scaled (see section 2.3) or interpolated to a spatial resolution of 0.16° as climatic forcings. This resolution corresponds to the spatial resolution of the Climate Research Unit data (New *et al.*, 2002) used in the downscaling method (section 2.3). As mentioned previously LPJ-LMfire requires forcings with interannual variability. Since the downscaling procedure provides only a mean climatology we

use an anomaly procedure to build the forcing fields:

- We average the detrended version of a 20th Century Reanalysis climatology constructed by (Pfeiffer *et al.*, 2013), and increase its initial spatial resolution (0.5°) to 0.16° through a bilinear interpolation. We thus obtain a high-resolution mean present-day climate.
- We compute the anomaly between this mean present-day climate and the high resolution climatology from the IPSL_CM5A simulation.
- We add the anomaly to the detrended version of the 20th Century Reanalysis climatology. We therefore make the assumption that there has been no change in interannual variability, which is the best approach we could follow here given the available data. It would be interesting to test this hypothesis with high resolution regional climate models in a future work.

Lightening strike frequency is not simulated in IPSL_CM5A. For this variable we keep the time-series constructed by Pfeiffer *et al.* (2013) based on a modern dataset (Christian *et al.*, 2003) and on the convective available potential energy anomalies from the 20th Century reanalysis Project (Compo *et al.*, 2011) to account for interannual variability. Similarly, soil types are taken from the standard driver data set of Pfeiffer *et al.* (2013). Lightening and soil variables are simply bilinearly interpolated to 0.16°.

We perform 3 simulations of the southern African vegetation: a control simulation using the outputs of a present-day simulation of IPSL_CM5A and two MIS4 simulations, using the outputs of the MIS4_max and MIS4_min IPSL_CM5A simulations. The atmospheric CO₂ level is fixed at 310 ppm, 230 ppm and 200 ppm respectively. For MIS4 simulations, new land points appear along the coastal edges, due to the glacial sea-level reduction. For all variables, the standard input data of Pfeiffer *et al.* (2013) are extrapolated on these new points using the nearest continental neighbour.

Several forcing parameters change between the MIS4_min and MIS4_max LPJ-LMfire simulations: climate, insolation and atmospheric CO₂, which is known to impact vegetation through its impact on photosynthesis and respiration rates as well as on the plant water-use efficiency (e.g. Jolly & Haxeltine (1997); Cowling & Sykes (1999); Harrison & Prentice (2003); Prentice & Harrison (2009); Woillez *et al.* (2011)). To investigate the relative impact of these forcing factors, we perform 4 sensitivity experiments, hereafter labelled TEST_PRECIP, TEST_TEMP, TEST_CO2 and TEST_INSOL.

In TEST_PRECIP (resp. TEST_TEMP), we force LPJ-LMfire with the MIS4_max conditions, except for precipitation and the number of wet days (resp. the air temperature and the amplitude of the diurnal cycle) for which we take the values from MIS4_min. Thus, we isolate the impact of the change in precipitation (resp. temperature) alone when precession decreases. In TEST_CO2, LPJ-LMfire is forced with the MIS4_max climate, but with a CO₂ value of 200 ppm to isolate the impact of the CO₂ decrease between the beginning and end of MIS4. And finally, in TEST_insol we

force LPJ-LMfire with the climate of MIS4_max but impose the orbital parameters of MIS4_min:
this run tests the impact of solar insolation change alone on photosynthesis and thus on vegetation
200 productivity.

For all simulations, the model is spun up for 1080 years, to make sure that the vegetation is at
equilibrium with the climatic forcings. The analysis of the outputs are performed on averages over
the last 60 years of simulation.

205 2.3 Statistical downscaling

To increase the spatial resolution of the AOGCM outputs required to drive LPJ-LMfire at high reso-
lution over southern Africa, we chose to apply a downscaling method and use a Generalized Additive
Model (GAM). The advantages of GAM compared to other downscaling procedures has been shown
by Wilby *et al.* (1998). Here we follow the approach developed by Vrac *et al.* (2007) for Western
210 Europe.

The downscaling procedure has been performed using the statistical programming environment R
(R Development Core Team, 2009) and its "mgcv" package (Wood, 2006). The method has been
developed and evaluated for the downscaling of air temperature and precipitation (Vrac *et al.*, 2007;
Martin *et al.*, 2011; Levavasseur *et al.*, 2011). Here we also apply it for the downscaling of the
215 diurnal-cycle amplitude and number of wet days, which by nature are expected to behave simi-
lar to temperature and precipitation respectively. The downscaling method has not been tested for
cloudiness and wind speed, so these two variables were simply bi-linearly interpolated to the desired
0.16° spatial resolution.

220 GAM builds statistical relationships between local-scale observations (called *predictand*) and
large-scale variables (called *predictors*, generally from fields of climate models). The expectation of
the explained variable Y (the predictand) is computed by a sum of non-linear functions, defined as
cubic splines in our case, conditionally on the predictors X (Hastie & Tibshirani, 1990):

$$E(Y_i | X_{n,n=1\dots k}) = \beta_0 + \sum_{n=1}^k f_n(X_{i,n}) \quad (1)$$

225 where β_0 is the intercept, k the number of predictors and i the grid-cell.

Splines functions are piecewise third order polynomial functions, evaluated at four knots. Each
function has at most 12 parameters. Such a model has both a great flexibility and a (relatively)
limited number of parameters to compute (see Vrac *et al.* (2007) for more details).

To calibrate the GAM (i.e. to build the splines) we use the high-resolution gridded climatologies
230 from the Climate Research Unit (CRU) database (New *et al.*, 2002) as predictands. For each grid-
point, each dataset consists of twelve monthly means (average over the period 1961 to 1990) at

a regular spatial resolution of 0.16° in latitude and longitude, corresponding to our downscaling resolution. To use GAM as in equation (1), the distribution family of the explained variable is assumed to be Gaussian. Although temperature data classically satisfy this normality assumption, precipitation values have to be log-transformed before the calibration step (Cheng & Qi, 2002).

The predictors may be divided into two groups: the "physical" predictors and the "geographical" ones. The "physical" predictors are directly extracted from a 20th century IPSL_CM5A simulation (years 1961 to 1990) and depend on climate dynamics. The "geographical" predictors include geographical information such as topography and distance to the ocean. All the predictors must have the same spatial resolution as the predictands. Therefore, the IPSL_CM5A outputs used as predictors are bilinearly interpolated to 0.16° .

The statistical relationships are established only for a given region and cannot be applied to another. Therefore, we have performed different tests to select the appropriate combinations of predictors for southern Africa, which differ from the selection of Vrac *et al.* (2007) for Europe. The "optimal" predictors set is selected according to the Bayesian Information Criterion (BIC, Schwartz (1978)) as described by Vrac *et al.* (2007). The BIC allows selecting a statistical model (and the associated predictors) by balancing the risk of over-fitting.

To be evaluated in fair conditions, the GAM requires independent samples between the calibration and projection steps. This condition is not satisfied for the present day since we use the same IPSL_CM5A simulation for both steps. Therefore, following Levavasseur *et al.* (2011), we use a "cross-validation" procedure and do the calibration on 11 months and the projection on the remaining month. With a rotation of this month we are thus able to perform the projection step for any month based on an independent calibration data set.

To perform the downscaling for MIS4, we use the splines built for present-day and project with the MIS4 predictors (for both MIS4_max and MIS4_min experiments). If the predictors values for the MIS4 simulation are outside the calibration range, the spline is simply linearly extrapolated to cover the whole range of the new values.

3 Results and discussion

3.1 Downscaling results for present-day southern African climate

Our best predictors' combinations to downscale independently air temperature, diurnal-cycle amplitude, precipitation and number of wet days are listed in Tab.2 with their respective percentage of explained variance (i.e. the percentage of observed variance explained by a given set of explanatory variables, Saporta (1990)):

$$\% \text{ of variance explained} = \frac{\sum_i (y_i^* - \bar{y})^2}{\sum_i (y_i - \bar{y})^2} \times 100 \quad (2)$$

265 where y_i^* is the GAM-predicted value, y_i the observed value, and \bar{y} the observed mean.

As "physical" predictors we use air temperature at the surface, precipitation, relative humidity, diurnal-cycle amplitude and wind speed at 10 m. The "geographical" predictors are the topography and two continentality indexes. To account for the effect of local elevation on climate, we use the high-resolution gridded topography ETOPO2, from the National Geophysical Data Center (NGDC, 270 Amante & Eakins (2008)). For MIS4 we have added +70 m to this topography, to account for the reduced sea-level compared to present day. The first continentality index is the "diffusive" continentality (DCO), which represents the shortest distance to the ocean (e.g. 0% at the ocean edge and 100% very remote from any ocean, corresponding to a purely continental air parcel. For southern Africa, DCO reaches 100% about 300 km from the ocean.). The second continentality index is the 275 "advective" continentality (ACO). ACO is similar to DCO albeit being modulated by the large-scale wind intensities and directions simulated with IPSL_CM5A and represents an index of the continentalization of air masses. For more details about ACO and DCO the reader is referred to Levvasseur *et al.* (2011).

280 Fig.2 and Fig.3 illustrate the improvement of the present-day IPSL_CM5A temperature and precipitation outputs through the downscaling. When the mean annual temperature simulated with IPSL_CM5A for present-day is simply interpolated to 0.16° (Fig.2.b) the values are systematically lower than the CRU data (Fig.2.c), except in the eastern mountains, where the orographic effect is not correctly captured and the temperature is overestimated by 3-4°C. The downscaling method (Fig.2.c) 285 corrects this cool bias and better captures the temperature pattern on elevated regions (Fig.2.d). We obtain a very high percentage of variance explained for this variable (about 95%, see Tab.2). We also obtain satisfactory results for the amplitude of the diurnal cycle, with about 82% of the variance explained (Tab.2).

The comparison between the interpolated annual precipitation simulated by IPSL_CM5A and the 290 CRU data (Fig.3.b,c) show that the AOGCM strongly overestimates precipitation in the summer rainfall area (positive anomaly above 600 mm/year) and fails to simulate the austral winter precipitation in the South-West. The precipitation pattern obtained after downscaling (Fig.3.d,e) reduces both biases. The percentage of variance explained is however only 58.5% (Tab.2). This relatively low percentage is in the range of the explained variance values obtained by Martin *et al.* (2011) 295 for Europe. Capturing the precipitation pattern at a small spatial scale remains a challenge, given the spatially variable nature of precipitation, thus we did not expect to reach a higher percentage of explained variance.

The downscaling procedure assumes that the statistical relationships established for present-day 300 climate are stationary in time and remain valid for different periods. This assumption may be questionable in a paleoclimatic context (Vrac *et al.*, 2007), particularly if the values of the predictors

are outside the calibration range. In our case, most of the predictors' values for MIS4_max and MIS4_min are still within the range of calibration, thus bringing confidence on the validity of the statistical relationships for that period. Some of the MIS4 monthly temperature values simulated by IPSL-CM5A are lower than the calibration values by a few °C, corresponding to the austral winter temperatures in the center of southern Africa, but the splines constructed by the GAM for this predictor are roughly linear and a linear extrapolation should not lead to unrealistic projections (see Fig.S2 in the Supplement). We are therefore confident that the method can reasonably be applied for the downscaling of the MIS4 climate over southern Africa.

3.2 Simulation of present-day vegetation and fire activity over southern Africa

3.2.1 Vegetation

The different biomes currently present in southern Africa have been initially described and classified by White (1983). This first classification has been revisited by Rutherford (1997), Scholes (1997) and Mucina *et al.* (2007). Urrego *et al.* (2014) combine the classification of Scholes (1997) and Mucina *et al.* (2007) and distinguish 8 different biomes: desert, Nama Karoo and Succulent Karoo (semi-desert) in the West and Central regions, *Fynbos* (Mediterranean hard-leaf scrubs) in the southern coastal regions, grasslands in the East, broad-leaved savanna in the North, fine-leaved savanna in the North and central West, and forest in the eastern coastal regions (Fig.4.a).

In order to evaluate the performances of LPJ-LMfire for present-day, we compare qualitatively the vegetation simulated in the control present-day run, given as fractions of grid-cell occupied by the different PFTs, (Fig.4.b) to the modern biome distribution (Fig.4.a).

LPJ-LMfire simulates high bare ground fractions in the North-West, above 50% West of 24°E and North of 32°S (Fig.4.b), corresponding roughly to the desert and Karoo regions (Fig.4.a). The center of the sub-continent is occupied by a mixture of bare soil, grass and trees. High grass fractions are simulated in the South and South-West. On the eastern side and southern coast, including the Cape region, the model simulates forest fractions above 50% (Fig.4.b), composed mainly of temperate woody PFTs.

The distribution of the simulated vegetation strongly depends on the annual precipitation (Fig.5). The fraction of bare soil (trees) decreases (increases) somewhat linearly when annual precipitation increases (decreases). The grass fractions globally increase with annual precipitation between 0 and 600 mm/year and decrease for wetter conditions, replaced by trees which are more competitive. We can distinguish two peaks in the grass fractions, around annual precipitation values of 300 mm/year and 600 mm/year. The first peak corresponds to the hinterland of the Cape region, where precipitation occurs during the austral winter, and the second one reflects the gradual increase and decrease of grass fractions from the West to the East of southern Africa (Fig.4.a).

The presence of forests in the Cape region disagrees with observations, since the region is actually

covered by the mediterranean-like scrub Fynbos (Fig.4.a). This bias was expected since LPJ-LMfire does not simulate shrubs. The simulated extension of forests on the eastern side is overestimated, the region being dominated today by grasslands and savanna and forest being limited to a coastal band along the Indian Ocean. This bias is also present when LPJ-LMfire is forced with the original dataset of Pfeiffer *et al.* (2013), based on observations and reanalyses (data not shown), and therefore can be attributed to the DGVM itself rather than to biases in the climatic forcings from IPSL_CM5A.

The overestimation of trees and underestimation of grasses compared to observations could be due either to intrinsic biases of the DGVM, or to the anthropogenic influence on the modern southern African vegetation. The diverse parameterizations used in the simulation of processes governing vegetation dynamics or in the fire module may not be optimal for southern Africa, especially at high spatial resolution. In a similar simulation performed over Europe (data not shown) the model results show the same type of biases and overestimates forests in the Mediterranean region, which suggests that the impact of a large amplitude in the hydrological seasonal cycle on vegetation is not adequately simulated in the model. The impact of fire on trees development, which has been suggested to be a determining factor in southern Africa (Westfall *et al.*, 1983; Titshall *et al.*, 2000; Bond *et al.*, 2003a,b), may also be underestimated. The improvement of the model calibration may be possible, but requires further tests and comparisons with observation data at local scale from regions without current anthropogenic impact, such as National parks.

Indeed, the model simulates the potential vegetation, i.e. without any anthropogenic disturbance such as agriculture, farming, impact on the fire regime through anthropogenic ignition or fire suppression, or spreading of alien plants (for more details on human impact on fire regimes in Africa, see Archibald *et al.* (2009, 2012). The modern landscape could be at least partly the result of human activities (Pfeiffer *et al.*, 2013). This hypothesis is supported by pollen data from the marine core MD96-2048, off eastern southern Africa (Dupont, 2011), which show higher percentages of tree pollen during the last interglacial, when human impact was likely negligible.

3.2.2 Fire

For present-day, LPJ-LMfire simulates fires mainly in the center of southern Africa, between 23-27°E, and in the South, between 31-33°S. In these two regions, annual burned area fractions are around 20-30% and 30-40% respectively (Fig.6.a). In other words, fires occur outside the desert region on the West side, where fuel load is too small to sustain fires, and outside the regions where humidity and tree fractions are high (Fig.4.b).

Fig.6.b shows the annual fraction of a grid-cell burned plotted against annual precipitation. The model simulates 2 peaks in fire activity, around 300 and 600 mm/year, corresponding to the grid-cells with the maximum fractions of grass (Fig.5.b). For precipitation above 600 mm/year, the burned fractions steeply decrease, reflecting the lower fire activity for wetter conditions and high tree fractions. Below 300 mm/year, fire activity also decreases, following the decrease in available

fuel load.

The maximum burned area fractions simulated with LPJ-LMfire are about three to four times
375 higher than modern observations of fire activity in southern Africa: for the period 1997-2011, the
average annual burned area fractions are below 5% (Giglio *et al.* (2010), <http://globalfiredata.org>,
data for southern Africa shown on Fig.S3 in the Supplement).

Our results are in agreement with Pfeiffer *et al.* (2013) without agricultural land cover. If agricul-
ture is taken into account and lightning-caused fires are excluded from the cultivated areas, results
380 are in good agreement with observations (Pfeiffer *et al.* (2013)), which suggests a strong influence
of human activity through agriculture on the modern fire regime of southern Africa. The overesti-
mation of annual burned fractions in southern Africa in our simulations can thus be attributed to the
absence of agricultural land use and does not prevent the analysis of the response of the fire regime
to paleoclimatic changes.

385 3.3 Climate, vegetation and fire response to precession changes for MIS4 conditions

3.3.1 Climate

Here we focus on the temperature and precipitation changes when precession decreases for MIS4
boundary conditions (MIS4_min - MIS4_max) over Africa. The mean features of the temperature
and precipitation anomalies at global scale simulated in MIS4_max compared to present-day can
390 be found in the supplementary data (Fig.S4 in the Supplement). Here we focus on the temperature
and precipitation changes when precession decreases for MIS4 boundary conditions (MIS4_min -
MIS4_max) over Africa.

The increase in boreal summer insolation (JJA) in the northern hemisphere (Fig.1) leads to higher
temperatures over Africa North of 30°N (Fig.7.a) and to the intensification of the North African
395 monsoon in response to the enhancement of the land-sea temperature contrast. Precipitation over
Sahel is intensified and shifted northward, due to the enhancement of the monsoon winds. Precip-
itation around 4°N decreases as moisture is advected more inland, whereas we observe a positive
precipitation anomaly around 10°N. The negative anomaly in temperature in the same latitude band
is caused by the increase in the latent heat flux associated to the wetter conditions. The mechanism
400 described here is qualitatively similar to the simulation results of Marzin & Braconnot (2009b) for
the Holocene. We leave the detailed investigation of the differences in the North African monsoon
sensitivity to precession for the Holocene or MIS4 boundary conditions for another study. We simply
point out here the persistence of the mechanism for the MIS4 glacial conditions.

During the austral summer (DJF) the negative insolation anomaly over both hemispheres in MIS4_min
405 compared to MIS4_max (Fig.1) leads to a global cooling over Africa (Fig.7.b), ranging from -1°C
to -4°C, depending on the region considered. For precipitation, the model simulates drier conditions
south of 5°N, over the regions under the influence of the ITCZ during DJF. This drying can be linked

to the lower temperatures, causing a decrease in the intensity of the convection. Thus, our results show an opposite response of the North African monsoon and the southern African monsoon to precession changes, at least for the MIS4 glacial boundary conditions.

After downscaling, the climate simulated in southern Africa in the summer rainfall region (eastern part) for MIS4_max is drier than the modern one, with total annual rainfall anomalies between -50 and -300 mm/year (Fig.8.a). The decrease of precession (MIS4_min - MIS4_max) leads to an additional drying in the East (-100 to -200 mm/year over most part of the summer rainfall area) and in the center (-50 to -100 mm/year around 22°E) (Fig.8.b). Fig.9 presents the annual cycle of the downscaled temperature and precipitation over the area of summer rainfall (DJF) for MIS4_max and MIS4_min. The precession decrease leads to a decrease of the amplitude of the seasonal cycle of both temperature and precipitation. The austral summer (DJF) is drier and cooler, with a maximum precipitation decrease in December and January of 40 and 35 mm/month respectively, i.e. a decrease of 37 and 46%. The drying is accompanied by a 3°C cooling in the monthly temperature. No significant changes in precipitation or temperatures occur during the winter months (JJA).

Our results confirm a strong impact of precession on the hydrological cycle of the region. The simulations results are in qualitative agreement with the data from the Pretorian Saltpan, in the North of southern Africa (Partridge *et al.*, 1997; Kristen *et al.*, 2007). The analysis of the lacustrine sediments from this site, covering the last 200 000 years, show periodic variations between wet and dry periods at the precessional frequency (23 ky). However, absolute dating, based on radio-carbon analysis, only covers the first 43 ky of the sequence, preventing the determination of a precise phasing relationship between rainfall and precession changes. Kristen *et al.* (2007) have suggested that precipitation changes at Pretorian Saltpan could be related to changes in the intensity and/or the length of the rainy season in that region. Our IPSL_CM5A simulations does not show changes in the length of the rainy season when precession decreases, but rather a flattening of the hydrological cycle with less intense rainfall from November to March. Partridge *et al.* (1997) have estimated the sensitivity of the southern African summer rainfall to insolation changes to 4.5 (i.e. 1% increase in summer insolation produces 4.5% precipitation increase). The annual downscaled precipitation in the region of the Pretorian Saltpan in MIS4_min and MIS4_max are 615 mm/year and 770 mm/year respectively, corresponding to a summer insolation at 30°S of 463 W/m² and 495 W/m², i.e. a 25% precipitation increase for 7% insolation increase. The precipitation sensitivity coefficient computed from these values is thus 3.5, smaller than the results of Partridge *et al.* (1997) but of the same order of magnitude. However, even when the record from Pretorian Saltpan is tuned on the precession variations, the reconstructed precipitation at Pretorian Saltpan and insolation at 30°S diverge after 60 kyr. Our simulations thus correspond to the very last period where precession and summer rainfall in southern Africa seem to co-vary. However, since we performed only snapshot simulations, we cannot

investigate the possible leads and lags between precession and precipitation changes to validate or invalidate the tuning of Partridge *et al.* (1997). AOGCMs are not suitable tools to investigate this issue, given their high computational cost. Simulations with faster AOGCMs would be required to perform transient runs and to investigate further the links between precession and precipitation in southern Africa over several precession cycles.

3.3.2 Vegetation changes in southern Africa

The vegetation pattern simulated over southern Africa for MIS4_max (Fig.10.a) is close to the one simulated for present-day (Fig.4.b), with high tree fractions in the East. The high tree percentages in that region seem to be more in qualitative agreement with pollen data for MIS4 than for present day. Indeed, pollen data from marine core MD96-2048 (off the eastern southern African coast, Dupont (2011)) show about 40% of tree pollen at the beginning of MIS4 vs about 20% for present day. This observation suggests that part of the present day mismatches between the vegetation model and actual observations might indeed be attributed to anthropogenic effects (section 3.2.1).

In MIS4_min (Fig.10.b,c) bare soil fractions increase southwards and eastwards, at the expense of grasses and trees. In the center of southern Africa (22° - 28°E) the model simulates increases in the bare soil fractions between 10-25%. An increase of similar magnitude also occurs in the South-West. Decreases in tree fractions (between 5 and 25%) occur on all grid-cells where they are present in MIS4_max (Fig.10.c). The total decrease in the area occupied by trees over southern Africa is between about 18-19% for the evergreen woody PFTs and 30% for the summergreen (Fig.11.a). Grass fractions decrease by 5-15% in the center and South-West but increase in the East and South, at the expense of trees (Fig.10.c). Overall, the total area covered by grasses over southern Africa decreases by about 7% (Fig.11.a).

The simulated increase in the bare soil fractions can be considered as a desertification of the landscape and is in qualitative agreement with pollen data off West southern Africa (marine core MD96-2098), which show an expansion in the semi-desert biomes (Urrego *et al.*, 2014) when precession decreases during MIS4. Likewise, our results are in agreement with the increase in arboreal pollen off East southern Africa during the same period (marine core MD96-2048, Dupont (2011)).

The results of the sensitivity runs are synthesized on Fig.11.a which shows the percentages of change in the total area occupied by the different PFTs for each simulation compared to MIS4_max.

The diagrams show that relative impact of the different factors that we tested (precipitation, temperature, CO₂ and insolation) depends on the PFT:

- **Trees:** The CO₂ decrease between MIS4_max and TEST_CO2 is only 30 ppm, but is responsible for a decrease between 3% and 7% for the 3 woody PFTs. This result is not very surprising given that LPJ is a DGVM rather sensitive to CO₂ concentrations (e.g. Köhler *et al.* (2005)).

Temperature changes alone (TEST_TEMP) lead to an increase of the Temperate needleleaf

evergreen trees and the temperate broadleaf evergreen trees of +11% and +4.5% respectively but to a small decrease of the temperate broadleaf summergreen trees (-5%). Changes caused by insolation changes (TEST_INSOL) are smaller than 3% for the 3 temperate woody PFTs. The changes simulated in TEST_PRECIP are close to the changes obtained for MIS4_min compared to MIS4_max.

- **Grasses:** The changes in the total area occupied by grasses for MIS4_min compared to MIS4_max is about -7%. The changes simulated in the different sensitivity runs compared to MIS4_max are small, with less than 1% of variations in TEST_PRECIP and TEST_TEMP and about -3% in TEST_CO2 and TEST_INSOL

Precipitation changes alone are sufficient to simulate a decrease in the surfaces occupied by the woody PFTs similar to the decrease obtained for MIS4_min. Precipitation changes thus appear as the main factor driving the changes in tree fractions when precession decreases (MIS4_min - MIS4_max). The relative impact of temperature, insolation and CO₂ changes between MIS4_min and MIS4_max compensate each other. The sensitivity of grasses at the scale of southern Africa as a whole to the different factors tested is less clear. In particular, contrary to the woody PFTs, grasses seem to be insensitive to precipitation changes. However, this result hides important spatial differences between the East, where grasses increase with precession decrease and the central areas, where grass fractions decrease (Fig.10). In the eastern part, precipitation decrease is the main driver of grasses expansion (Fig.11.b). In the center, the total decrease in grass surface is about -22%. Precipitation changes alone lead to a decrease of -10% and the CO₂ decrease to a decrease of -7%. These differences in the response of grass between the East and the center of southern Africa can be explained by the vegetation dynamics and the competitiveness with the woody PFTs. In the East, the precipitation decrease drives the regression of trees but grasses have smaller water requirements and can expand on the space left by the woody PFTs. In the center, where annual precipitation is lower, the drying of climate affects both grasses and trees and the first driver of the regression of grasses is the precipitation decrease. However, the impact of the CO₂ decrease is of similar magnitude and appears as an important factor to explain grass changes.

3.3.3 Fire activity changes in southern Africa

Fig.12 shows changes in the percentages of grid-cell burned annually when precession decreases (MIS4_min - MIS4_max). The LPJ-LMfire model simulates a decrease in fire activity in the center of southern Africa (-5 to -20%) and an increase in the East and South (+5 to +10%). The comparison between Fig.12 and Fig.10 shows that fire activity increases when grass fractions increase and decreases where grass and/or tree fractions decrease. As mentioned in the previous section, the grass increase in the East and South merely reflects the regression of trees and is therefore strongly dependent on the vegetation initial state in MIS4_max.

To better visualize this relationship between vegetation changes and fire activity we have plotted the changes in bare soil, tree and grass fractions against changes in the annual burned surface on Fig.13.a. The graph clearly shows a decrease in burned fractions over grid-cells where bare soil fractions increase and tree and grass fractions decrease, and an increase in burned fractions with higher grass fractions (Fig.13.a). On the contrary, no clear relationship appears between the amplitude of the annual precipitation changes and the fire activity (Fig.13.b). This can be attributed to a different vegetation response in the East and in the Center of southern Africa. In the East, despite the precipitation decrease the climate is still wet enough to allow an increase of grass (i.e. easily incinerable fuels), whereas in the center the climate has become too dry and grasses decline, leading to smaller amounts of light fuel and a decrease of fire.

At the scale of the whole southern Africa, the dominant signal is the regression of grass-fueled fires in response to the precipitation decrease in the summer rainfall area, in qualitative agreement with Daniau *et al.* (2013). The simulations confirm the link between precession and fire activity, inferred from the micro-charcoal record. As discussed in Daniau *et al.* (2013), the record can reflect either shifts in grassland extent or shifts in grassland productivity. Daniau *et al.* (2013) conclude that the latter hypothesis was the most likely. Our modeling results support this conclusion. Indeed, LPJ-LMfire simulates changes in vegetation fractions mainly limited to 5-15% for trees and 5-10% for grasses (Fig.10.c) in most parts of southern Africa. Such percentages reflect changes in the productivity and density of the PFTs, but are not large enough to be interpreted as biome shifts.

Our results suggest that precession decrease appears to impact fire activity mainly indirectly, via changes in fuel load, rather than directly via changes in humidity. It confirms that vegetation response to climate changes have to be taken into account to investigate fire changes and highlight the importance of fuel load and how increased dryness can paradoxically lead to a decrease in fire activity in southern Africa.

Such a conclusion has been previously suggested for the last 21 kyr (Turner *et al.*, 2008) and during the Last Glacial period (Daniau *et al.*, 2007) in the Mediterranean region.

4 Conclusions

We have performed two simulations of the MIS4 climate with the AOGCM IPSL_CM5A, for a maximum and minimum of the climatic precession index, and analyzed the simulated climatic changes over Africa, with a focus on southern Africa. The decrease of the precession index leads to an increase of boreal summer insolation in the North hemisphere and to an intensification of the North African monsoon. On the contrary, insolation decrease during austral summer lead to a cooling over Africa and to a decrease in the convective activity associated to the ITCZ, leading to a decrease

of precipitation over the regions under its influence, including the East of southern Africa. Thus, our results show an anti-correlation between the North and South African monsoons in response to precession changes for the MIS4 glacial boundary conditions.

The IPSL_CM5A outputs have been statistically downscaled or interpolated to obtain high resolution fields. These fields are used as input for the dynamic vegetation model LPJ-LMfire, to simulate vegetation and fire changes over southern Africa in response to precession changes.

The simulated potential present-day vegetation presents some biases compared to observations, but the model-data discrepancies are probably mostly due to the anthropogenic impact on the modern southern African vegetation. For our MIS4 vegetation simulations we can achieve the following conclusions, in qualitative agreement with observations: i) Precession decrease leads to a decrease of precipitation during austral summer in eastern southern Africa (summer rainfall area). No significant precipitation changes occur during the dry season. ii) The dryness increase causes an expansion of bare soil, which can be interpreted as a desertification, and a decrease in trees and grass fractions in the center of southern Africa. In the East, the model simulates an expansion of grasses in response to the precession decrease, due to their development on grid-cells where tree cover declines. iii) The simulated fire activity over southern Africa is strongly dependent on the vegetation type (i.e. fuel load) and decreases (increases) on grid-cells where grass fractions decrease (increase).

The results provided here show important climatic and environmental changes in southern Africa between the beginning and end of MIS4. How they could have affected the early human populations in that region could be tackled through ecological niche modeling (Banks *et al.*, 2008). However, our simulations do not take into account the impact of millennial-scale variability, which superimposes to the long-term orbitally driven climatic changes and was recently suggested as a driver of technological innovations (Ziegler *et al.*, 2013). This issue requires supplementary runs with the IPSL_CM5A model, similar to the freshwater-hosing experiments which have been performed with the older version of the GCM and for Last Glacial Maximum conditions (Kageyama *et al.*, 2009; Woillez *et al.*, 2013).

Acknowledgements. The present manuscript is a contribution to TRACSYMBOLS project, supported by the European research Council, TRACSYMBOLS no. 249587. This work also benefited from the HPC resources of CCRT and IDRIS made available by GENCI (Grand Equipement National de Calcul Intensif), CEA (Commissariat à l’Energie Atomique et aux Energies Alternatives) and CNRS (Centre National de la Recherche Scientifique). We thank Olivier Marti for his help in the construction of the correct boundary conditions for the GCM, and Jed Kaplan for providing the LPJ-LMfire model.

References

- Amante, C. & Eakins, B. (2008). Etopo1–1 arc-minute global relief model: procdures, data sources and anal-
 585 ysis. Technical report, National Geophysical Data Center, NESDIS, NOAA, US Department of Commerce,
 National Geophysical Data Center, Boulder, Colorado.
- Archibald, S., David, R., Van Wilgen, B., & Scholes, R. (2009). What limits fire ? an examination of drivers of
 burnt area in southern africa. *Global Change Biology*, **15**(3), 613–630.
- Archibald, S., Scholes, R., Roy, D., Roberts, G., & Boschetti, L. (2010). Southern African fire regimes as
 590 reaveled by remote sensing. *Journal of Wildland Fire*, **19**(7), 861–878.
- Archibald, S., Staver, A., & Levin, S. (2012). Evolution of human-driven fire regimes in africa. *PNAS*, **109**(3).
- Argus, D. & Peltier, W. (2010). Constraining models of postglacial rebound using space geodesy: a detailed
 assessment of model ICE-5G (VM2) and its relatives. *Geophysical Journal International*, **181**(2), 697–723.
- Banks, W., d’Errico, F., Townsend Peterson, A., Vanhaeren, M., Kageyama, M., Sepulchre, P., Ramstein, G.,
 595 Jost, A., & Lunt, D. (2008). Human ecological niches and ranges during the LGM in Europe derived from
 an application of eco-cultural niche modeling. *Journal of Archeological Science*, **35**(2), 481–491.
- Bond, W., Midgley, G., & Woodward, F. (2003a). The importance of low atmospheric CO₂ and fire in promoting
 the spread of grasslands and savannas. *Global Change Biology*, **9**, 973–982.
- Bond, W., Midgley, G., & Woodward, F. (2003b). What controls South African vegetation - climate or fire ?
 600 *South African Journal of Botany*, **69**(1), 79–91.
- Braconnot, P. & Marti, O. (2003). Impact of precession on monsoon characteristics from coupled ocean at-
 mosphere experiments: changes in Indian monsoon and Indian ocean climatology. *Marine Geology*, **1–3**,
 23–24.
- Braconnot, P., Joussaume, S. de Noblet, N., & Ramstein, G. (2000). Mid-Holocene and last glacial maximum
 605 African monsoon changes as simulated within the Paleoclimate modelling intercomparison project. *Global
 Planetary Changes*, **26**(1–3), 51–66.
- Cheng, M. & Qi, Y. (2002). Frontal Rainfall-Rate Distribution and some conclusions on the threshold method.
Journal of Applied Meteorology, **41**, 1128–1139.
- Christian, H., Blakeslee, R., Boccippio, D., Boeck, W., Buechler, D., Driscoll, K., Goodman, S., Hall, J.,
 610 Koshak, W., Mach, D., & Stewart, M. (2003). Global frequency and distribution of lightening as observed
 from space by the optical transient detector. *Journal of Geophysical Research: Atmospheres*(1984–2012),
108, ACL 4–1–ACL 4–15.
- Compo, G., Whitaker, J., Sardeshmukh, P., Matsui, N., Allan, R., Yin, X., Gleason, B., Vose, R., Rutledge, G.,
 Bessemoulin, P., Brönnimann, S., Brunet, M., Crouthamel, R., Grant, A., Groisman, P., Jones, P., Kruk, M.,
 615 Kruger, A., Marshall, G., Maugeri, M., Mok, H., Nordli, e., Ross, T., Trigo, R., Wang, X., Woodruff, S., &
 Worley, S. (2011). The Twentieth Century Reanalysis Project. *Quaterly Journal of the Royal Meteorological
 Society*, **137**(654), 1–28.
- Cowling, R., Richardson, D., & Pierce, S., editors (1997). *Vegetation of Southern Africa*. Cambridge University
 Press.
- 620 Cowling, S. & Sykes, M. (1999). Physiological significance of low atmospheric CO₂ for plant-climate interac-
 tions. *Quaternary Research*, **52**(2), 237–242.
- Daniau, A.-L., Sanchez-Goñi, M.-F., Beaufort, L., Laggoun-Défarge, F., Loutre, M.-F., & Duprat, J. (2007).

Dansgaard-Oeschger climatic variability revealed by fire emissions in southwestern Iberia. *Quaternary Science Reviews*, **26**(9–10), 1369–1383.

- 625 Daniau, A.-L., Sánchez-Gómez, M.-F., Martínez, P., Urrego, D., Bout-Roumazeilles, V., Desprat, S., & Marlon, J. R. (2013). Orbital-scale climate forcing of grassland burning in southern Africa. *PNAS*, **110**(13), 5069–5073.

d’Errico, F. & Henshilwood, C. (2007). Additional evidence for bone technology in the southern African middle stone age. *Journal of Human Evolution*, **52**, 142–163.

- 630 Dufresne, J.-L., Foujols, M.-A., Denvil, S., Caubel, A., Marti, O., Aumont, O., Balkanski, Y., Bekki, S., Bellenger, H., Benshila, R., Bony, S., Bopp, L., Braconnot, P., Borckmann, P., Cadule, P., Cheruy, F., Codron, F., Cozic, A., Cugnet, D., de Noblet, N., Duvel, J.-P., Ethé, C., Fairhead, L., Fichefet, T., Flavoni, S., Friedlingstien, P., Grandpeix, J.-Y., Guez, L., Guilyardi, E., Hauglustaine, D., Hourdin, F., Idelkadi, A., Ghattas, J., Joussaume, S., Kageyama, M., Krinner, G., Labetoulle, S., Lahellec, A., Lefebvre, M.-P., Lefevre, F., Levy, C., Li, Z., Lloyd, J., Lott, F., Madec, G., Mancip, M., Marchand, M., Masson, S., Meurdesoif, Y., Mignot, J., Musat, I., Parouty, S., Polcher, J., Rio, C., Schultz, M., Swingedouw, D., Szopa, S., Talandier, C., Terray, P., Viovy, N., & Vuichard, N. (2013). Climate change projections using the IPSL-CM5 Earth system model with an emphasis on changes between CMIP3 and CMIP5. *Climate Dynamics*, **40**(9–10), 2123–2165.

Dupont, L. (2011). Orbital scale vegetation change in Africa. *Quaternary Science Reviews*, **30**, 3589–3602.

- 640 Fichefet, T. & Morales-Maqueda, A.-M. (1997). Sensitivity of a global sea ice model to the treatment of ice thermodynamics and dynamics. *Journal of Geophysical Research*, **102**, 12609–12646.

Fichefet, T. & Morales-Maqueda, A.-M. (1999). Modelling the influence of snow accumulation and snow-ice formation on the seasonal cycle of the antarctic sea-ice cover. *Climate Dynamics*, **15**, 251–268.

- Gasse, F. (2000). Hydrological changes in the African tropics since the Last Glacial Maximum. *Quaternary Science Review*, **19**(1–5), 189–211.

Giglio, L., Randerson, J., van der Werf, G., Kasibhatla, P., Collatz, G., Morton, D., & DeFries, R. (2010). Assessing variability and long-term trends in burned area by merging multiple satellite fire products. *Biogeosciences*, **7**.

- Harrison, S. & Prentice, C. (2003). Climate and CO₂ controls on global vegetation distribution at the last glacial maximum : analysis based on palaeovegetation data, biome modelling and palaeoclimate simulations. *Global Change Biology*, **9**, 983–1004.

Hastie, T. & Tibshirani, R. (1990). *Generalized Additive Models*. London: Chapman and Hall.

- Henshilwood, C., d’Errico, F., Yates, R., Jacobs, Z., Tribolo, C., Duller, G., Mercier, N., Sealy, J., Valladas, H., Watts, I., & Wintle, A. (2002). Emergence of modern human behavior: middle stone age engravings from South Africa. *Science*, **295**, 1278–1280.

Henshilwood, C., d’Errico, F., & Watts, I. (2009). Engraved ochres from the middle stone age levels at Blombos Cave. South Africa. *Journal of Human Evolution*, **57**, 27–47.

- Hourdin, F., Musat, I., Bony, S., Braconnot, P., Codron, F., Dufresne, J.-L., Fairhead, L., Filiberti, M.-A., Friedlingstein, P., Grandpeix, J.-Y., Krinner, G., LeVan, P., Li, Z., & Lott, F. (2006). The LMDZ4 general circulation model: climate performance and sensitivity to parametrized physics with emphasis on tropical convection. *Climate Dynamics*, **27**, 787–813.

Jacobs, Z., Roberts, R., Galbraith, R., Deacon, H., Grün, R., Mackay, A., Mitchell, P., Vogelsang, R., & Wadley,

- L. (2008). Ages for the middle Stone age of southern Africa: implications for human behavior and dispersal. *Science*, **322**, 733–735.
- 665 Jolly, D. & Haxeltine, A. (1997). Effect of low glacial atmospheric CO₂ on tropical African montane vegetation. *Science*, **276**(5313), 786–788.
- Kageyama, M., Mignot, J., Swingedouw, D., Marzin, C., Alkama, R., & Marti, O. (2009). Glacial climate sensitivity to different states of the Atlantic Meridional Overturning Circulation: results from the IPSL model. *Climate of the Past*, **5**, 551–570.
- 670 Kageyama, M., braconnot, P., Bopp, L., Caubel, A., Foujols, M.-A., Guilyardi, E., Khodri, M., Lloyd, J., Lombard, F., Mariotti, V., Marti, O., Roy, T., & Woillez, M.-N. (2013a). Mid-Holocene and Last Glacial Maximum climate simulations with the IPSL model - part I: comparing IPSL_CM5A to IPSL_CM4. *Climate Dynamics*, **40**(9–10), 2447–2468.
- Kageyama, M., Braconnot, P., Bopp, L., Mariotti, V., Roy, T., Woillez, M.-N., Caubel, A., Foujols, M.-A.,
675 Guilyardi, E., Khodri, M., Lloyd, J., Lombard, F., & Marti, O. (2013b). Mid-Holocene and Last Glacial Maximum climate simulations with the IPSL model: part II: model-data comparisons. *Climate Dynamics*, **40**(9–10), 2469–2495.
- Köhler, P., Joos, F., Gerber, S., & Knutti, R. (2005). Simulated changes in vegetation distribution, land carbon storage, and atmospheric CO₂ in response to a collapse of the North Atlantic thermohaline circulation.
680 *Climate Dynamics*, **25**(7–8), 689–708.
- Krinner, G., Viovy, N., de Noblet-Ducoudré, N., J., O., Polcher, J., friedlingstein, P., Ciais, P., Sitch, S., & Prentice, I. C. (2005). A dynamic global vegetation model for studies of the coupled atmosphere-biosphere system. *Global Biogeochemical Cycles*, **19**.
- Kristen, I., Fuhrmann, A., Thorpe, J., Röhl, U., Wilkes, H., & Oberhänsli, H. (2007). Hydrological changes in
685 southern Africa over the last 200 Ka as recorded in lake sediments from the Tswaing impact crater. *South African Journal of Geology*, **110**, 311–326.
- Laskar, J., Robutel, P., Joutel, F., Gastineau, M., Correia, A., & Levrard, B. (2004). A long term numerical solution for the insolation quantities of the Earth. *Astronomy and Astrophysics*, **428**, 261–285.
- Levvasseur, G., Vrac, M., Roche, D., Paillard, D., Martin, A., & Vandenberghe, J. (2011). Present and LGM
690 permafrost from climate simulations: contribution of statistical downscaling. *Climate of the Past*, **7**, 1225–1246.
- Liu, Y., Stanturf, J., & Goodrick, S. (2010). Trends in global wildfire potential in a changing climate. *Forest Ecology and Management*, **259**, 685–697.
- Madec, G., Delecluse, P., Imbard, M., & Lévy, C. (1998). *OPA version 8.1 Ocean general circulation model reference manual*, page 91pp. Number 11. Note du Pole de Modélisation, Institut Pierre-Simon Laplace, Institut Pierre Simon Laplace, France.
- 695 Martin, A., Vrac, M., Paillard, D., Dumas, C., & Kageyama, M. (2011). Statistical-dynamical downscaling for Earth Models of Intermediate Complexity. *Submitted*.
- Marzin, C. & Braconnot, P. (2009a). The role of the ocean feedback on Asian and African monsoon variations
700 at 6 kyr and 9.5 kyr BP. *Comptes Rendus Geosciences*, **341**(8-9), 643–655.
- Marzin, C. & Braconnot, P. (2009b). Variations of Indian and African monsoons induced by insolation changes at 6 and 9.5 kyr BP. *Climate Dynamics*, **33**, 215–231.

- Masson, V., Braconnot, P., Jouzel, J., de Noblet, N., Cheddadi, R., & Marchal, O. (2000). Simulation of intense monsoons under glacial conditions. *Geophysical Research Letters*, **27**, 1747–1750.
- 705 Mucina, L., Rutherford, M., & Powrie, L. (2007). *Vegetation Map of South Africa, Lesotho and Swaziland, 2nd ed.* South African National Biodiversity Institute Pretoria.
- New, M., Lister, D., Hulme, M., & Makin, I. (2002). A high-resolution data set of surface climate over global land areas. *Climate Research*, **21**(1), 1–25.
- Oghaito, R. & Abe-Ouchi, A. (2007). The role of ocean thermodynamics and dynamics in Asian summer
710 monsoon changes during the Mid-Holocene. *Climate Dynamics*, **29**(1), 39–50.
- Partridge, T., Demenocal, P., Lorentz, S., Paiker, M., & Vogel, J. (1997). Orbital forcing of climate over South Africa: a 200,000-year rainfall record from the Pretorian Saltpan. *Quaternary Science Reviews*, **16**, 1125–1133.
- Petit, J., Jouzel, J., Raynaud, D., Barkov, N., Barnola, J., Basile, I., Bender, M., Chappellaz, J., Davis, M.,
715 Delaygue, G., Delmotte, M., Kotlyakov, V., Legrand, M., Lipenkov, V., Lorius, C., Pepin, L., Ritz, C., Saltzman, E., & Stievenard, M. (1999). Climate and atmospheric history of the past 420,000 years from the Vostok ice core, Antarctica. *Nature*, **399**(6735), 429–436.
- Pfeiffer, M., Spessa, A., & Kaplan, J. (2013). A model for global biomass burning in preindustrial time: LPJ-LMfire (v1.0). *Geoscientific Model Development*, **6**, 643–685.
- 720 Prentice, I. & Harrison, S. (2009). Ecosystem effects of CO₂ concentration: evidence from past climates. *Climate of the Past*, **5**, 297–307.
- Rutherford, M. (1997). *Categorization of biomes*. Vegetation of Southern Africa. Cambridge University Press, Cambridge, pp 91–98, ISBN 0-521-57142-1.
- Saporta, G. (1990). *Probabilités, Analyse des données et statistiques*. Editions Technip.
- 725 Scholes, R. (1997). *Savanna*, in Cowling, R.M., Richardson, D.M., Pierce, S.M. (Eds.), *Vegetation of Southern Africa*. Cambridge University Press, Cambridge, UK, pp.258–277.
- Schwartz, G. (1978). Estimating the dimension of a model. *The Annals of Statistics*, **6**, 461–464.
- Sitch, S., Smith, B., Prentice, I., Arneth, A., Bondeau, A., Cramer, W., Kaplan, J., Levis, S., Lucht, W., Sykes, M., Thonicke, K., & Venevsky, S. (2003). Evaluation of ecosystem dynamics, plant geography and terrestrial
730 carbon cycling in the LPJ dynamic global vegetation model. *Global Change Biology*, **9**(2), 161–185.
- Spahni, R., Chappellaz, J., Stocker, T., Loulergue, L., Hausammann, G., Kawamura, K., Flückiger, J., Schwander, J., Raynaud, D., Masson-Delmotte, V., & Jouzel, J. (2005). Atmospheric Methane and Nitrous Oxide of the Late Pleistocene from Antarctic Ice Cores. *Science*, **310**, 1317–1321.
- Thonicke, K., Spessa, A., Prentice, I., Harrison, S., Dong, L., & Carmona-Moreno, C. (2010). The influence
735 of vegetation, fire spread and fire behaviour on biomass burning and trace gas emissions: results from a process-based model. *Biogeosciences*, **7**, 1991–2011.
- Titshall, L., O'Connor, T., & Morris, C. (2000). Effect of long-term exclusion of fire and herbivory on the soils and vegetation of sour grassveld. *African Journal of Range and Forage Science*, **17**, 70–80.
- Turner, R., Roberts, N., & Jones, M. (2008). Climatic pacing of Mediterranean fire histories from lake sedimentary microcharcoal. *Global and Planetary Change*, **63**(4), 317–324.
- 740 Urrego, D., Sanchez-Goni, M.-F., Daniau, A.-L., Lechevrel, S., & Hanquiez, V. (2013). Increased aridity in southwestern africa during the last-interglacial warmest periods. *In progress*.

- Valcke, S. (2006). *OASIS3 user guide (prism_2-5)*. PRISM report no 2. Tech. rep. TR/CMGC/06/73, CERFACS, Toulouse, France, 60.
- 745 Vrac, M., Marbaix, P., Paillard, D., & Naveau, P. (2007). Non-linear statistical downscaling of present and LGM precipitation and temperatures over Europe. *Climate of the Past*, **3**, 669–682.
- Waelbroeck, C., Labeyrie, L., Michel, E., Duplessy, J.-C., McManus, J., Lambeck, K., Balbon, E., & Labracherie, M. (2002). Sea-level and deep water temperature changes derived from benthic foraminifera isotopic records. *Quaternary Science Reviews*, **21**, 295–305.
- 750 Wang, P., Clemens, S., Beaufort, L., Braconnot, P., Ganssen, G., Jian, Z., Kershaw, P., & Sarnthein, M. (2005). Evolution and variability of the Asian monsoon system: state of the art and outstanding issues. *Quaternary Science Review*, **24**(5–6), 595–629.
- Westfall, R., Everson, C., & Everson, T. (1983). The vegetation of the protected plots at Thabamhlope Research Station. *African Journal of Botany*, **2**, 15–25.
- 755 White, F. (1983). *The vegetation of Africa: a descriptive memoir to accompany the Unesco/AETFAT/UNSO vegetation map of Africa*. (Natural Resources Research: 20). Paris: United Nations Educational, Scientific and Cultural Organization 356p.
- Wilby, R., Wigley, T., Conway, D., Jones, P., Hewitson, B., Main, J., & Wilks, D. (1998). Statistical downscaling of general circulation model output: A comparison of methods. *Water Resources Research*, **34**(11), 2995–
- 760 3008.
- Willez, M.-N., Kageyama, M., Krinner, G., de Noblet-Ducoudré, N., Viovy, N., & Mancip, M. (2011). Impact of CO₂ and climate on the Last Glacial Maximum vegetation: results from the ORCHIDEE/IPSL models. *Climate of the Past*, **7**, 557–577.
- Willez, M.-N., Kageyama, M., Combourieu-Nebout, N., & Krinner, G. (2013). Simulating the vegetation
- 765 response in western Europe to abrupt climate changes under glacial background conditions. *Biogeosciences*, **10**, 1561–1582.
- Wood, S. (2006). *Generalized Additive Models: A introduction with R*. Chapman and Hall/CRC Press.
- Ziegler, M., Simon, M., Hall, I., Barker, S., Stringer, C., & Zahn, R. (2013). Development of middle stone age innovation linked to rapid climate change. *Nature Communications*, **4**(1905).

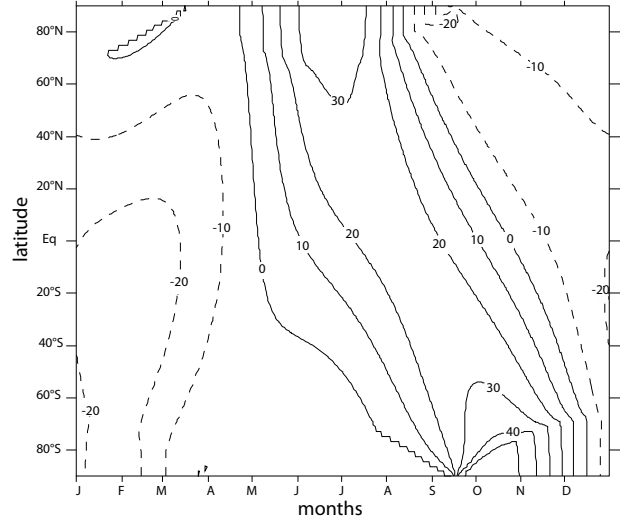


Fig. 1. Anomalies (MIS4_min-MIS4_max) in incoming solar radiation at the top of the atmosphere (W/m^2) averaged over the longitude and plotted as a function of months. The figure has been plotted based on the daily insolation values.

Table 1. Earth's orbital parameters and greenhouse concentrations values for the two MIS4 IPSL-CM5A simulations. ω stands for the longitude of the perihelion and e for the eccentricity.

Simulation name	eccentricity	obliquity	$\omega - 180$	precession index ($e \sin \omega$)	CO_2 (ppm)	CH_4 (ppb)	N_2O (ppb)
MIS4_max (-72 kyr)	0.02434	22.3907	80.09	0.01496	230	450	230
MIS4_min (-60 kyr)	0.01846	23.2329	266.65	-0.01785	200	426	230

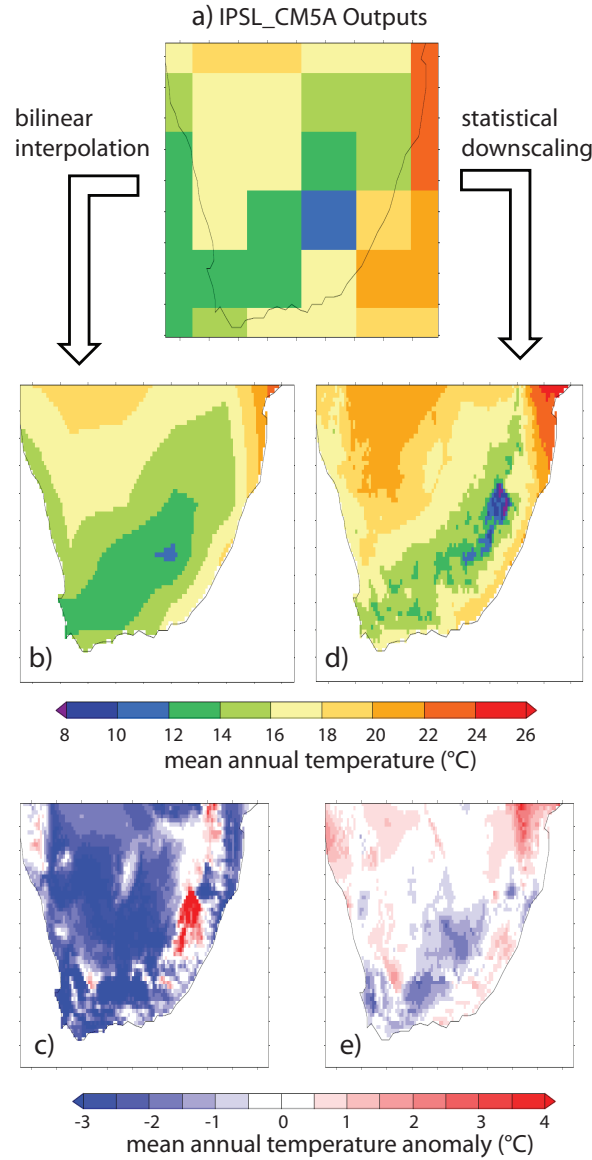


Fig. 2. a) Mean Annual temperature for present day simulated by IPSL_CM5A over southern Africa (Average over the years 1960 to 1990 from a 20th century simulation). Mean Annual temperature simulated by IPSL_CM5A for present-day with a spatial resolution increased to 0.16° through a bilinear interpolation (b) and difference with the CRU data (IPSL_CM5A - CRU) (c). Mean Annual temperature simulated by IPSL_CM5A for present-day with a spatial resolution increased to 0.16° through statistical downscaling (d) and difference with the CRU data (IPSL_CM5A - CRU) (e).

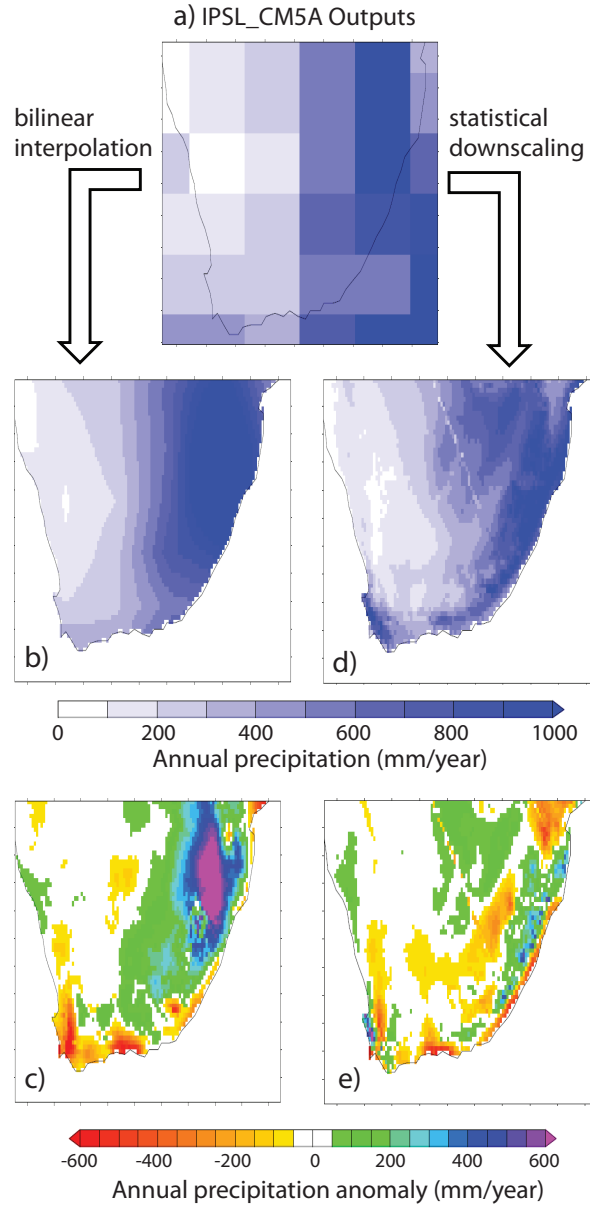
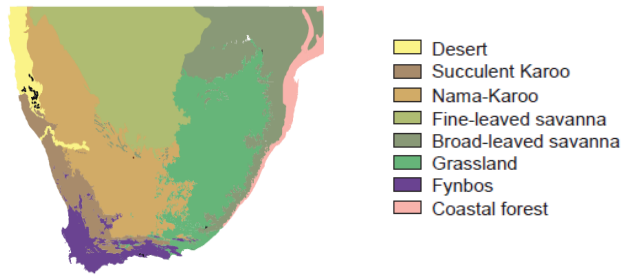


Fig. 3. a) Annual precipitation (mm/year) for present day simulated by IPSL_CM5A over southern Africa (Average over the years 1960 to 1990 from a 20th century simulation). Annual precipitation simulated by IPSL_CM5A for present-day with a spatial resolution increased to 0.16° through a bilinear interpolation (b) and difference with the CRU data (IPSL_CM5A - CRU)(c). Annual precipitation simulated by IPSL_CM5A for present-day with a spatial resolution increased to 0.16° through statistical downscaling (d) and difference with the CRU data (IPSL_CM5A - CRU) (e).

a) Observed modern biomes



b) LPJ-LMfire outputs

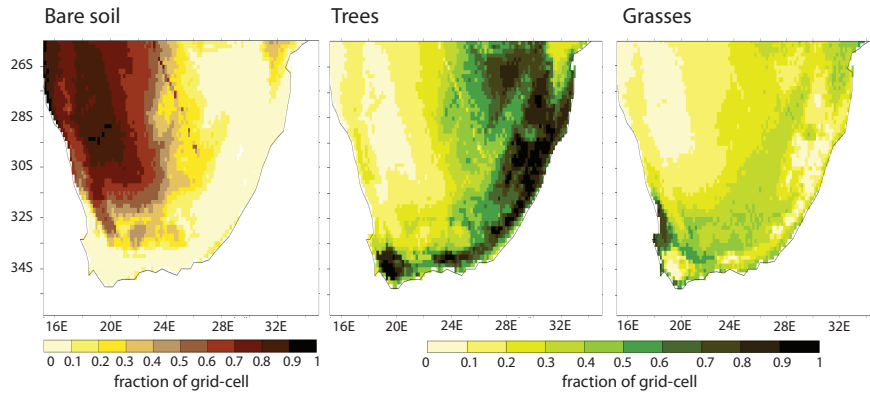


Fig. 4. a) Modern biomes of southern Africa (Scholes, 1997; Mucina *et al.*, 2007). b) Vegetation cover (Bare soil, trees and grass fractions) simulated with LPJ-LMfire forced off-line by the outputs of a present-day IPSL_CM5A simulation downscaled to 0.16° .

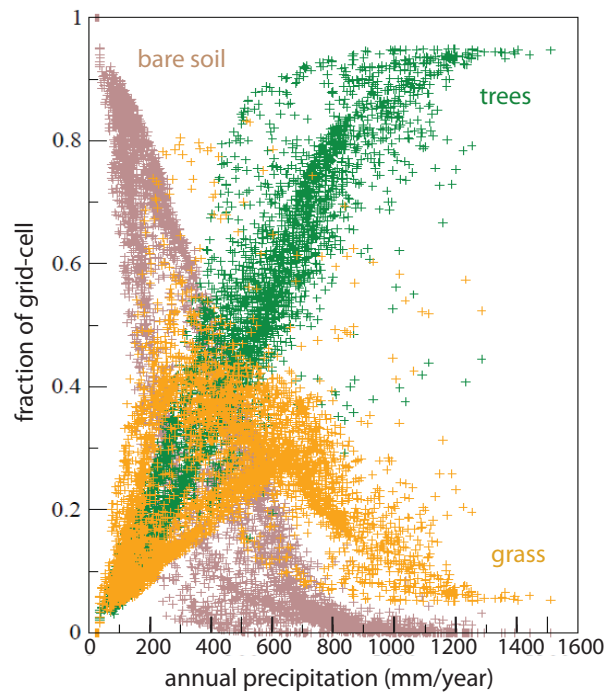


Fig. 5. Vegetation cover simulated for present day with LPJ-LMfire over southern Africa: Fraction of grid-cell occupied by bare soil (brown), trees (green) and grass (yellow) vs the total annual precipitation on the same grid-cell.

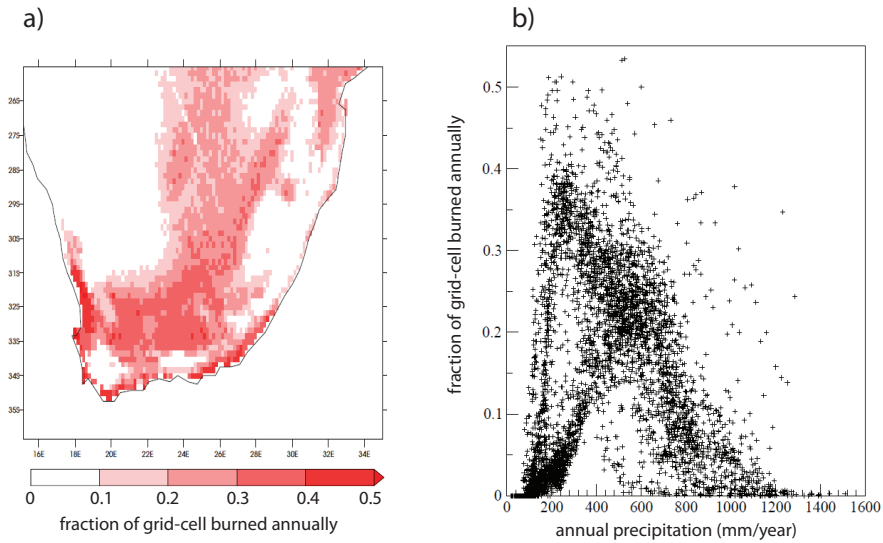
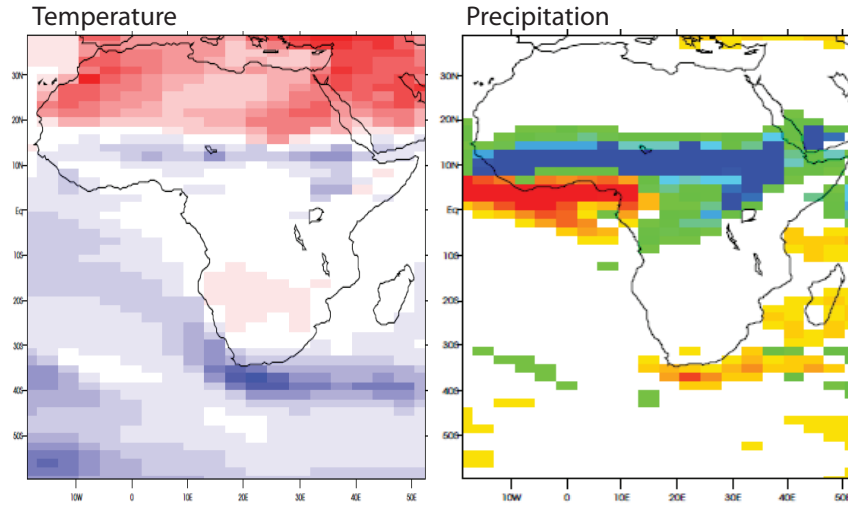


Fig. 6. Present-day simulation of fire activity over southern Africa with LPJ-LMfire. a) Fraction of grid-cell burned annually. b) Annual fraction of grid-cell burned vs total annual precipitation on the same grid-cell (mm/year).

Table 2. List of the predictors selected to perform the downscaling of monthly temperature and precipitation variables over southern Africa. The predictors "temperature", "relative humidity", "amplitude of the diurnal cycle", "precipitation" and "wind" are taken from the IPSL-CM5A simulation and interpolated to 0.16° . The diffusive continentality index corresponds to the shortest distance to the ocean; the advective continentality index depends on both the wind simulated in the GCM and the distance to the ocean. See Levavasseur *et al.* (2011) for a complete description of the construction of these two predictors.

Predictand	predictors	% of variance explained
Air temperature	Temperature, topography, diffusive continentality index	94.7
Amplitude of the diurnal cycle	Temperature, topography, relative humidity, amplitude of the diurnal cycle, diffusive continentality index	82.1
Precipitation	Temperature, advective and diffusive continentality indexes, precipitation, wind, topography	58.5
Number of wet days	Temperature, advective and diffusive continentality indexes, precipitation, wind, topography	88.5

a) MIS4_min - MIS4_max JJA



b) MIS4_min - MIS4max DJF

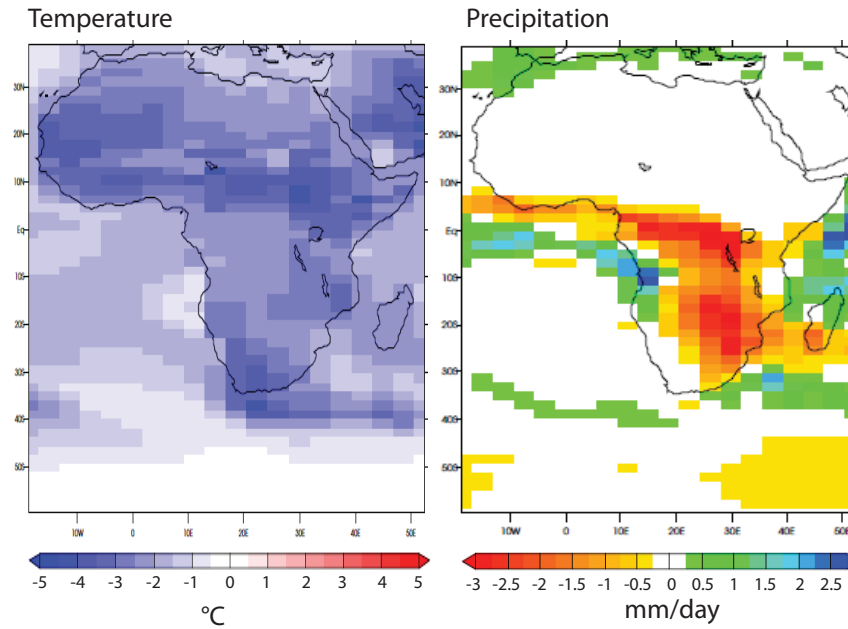


Fig. 7. Difference in mean temperature (°C) and mean precipitation (mm/day) simulated with IPSL_CM5A between the beginning and end of MIS4 (MIS4_min - MIS4_max). a) Average for the boreal summer month (June to August); b) average for the boreal winter months (December to February).

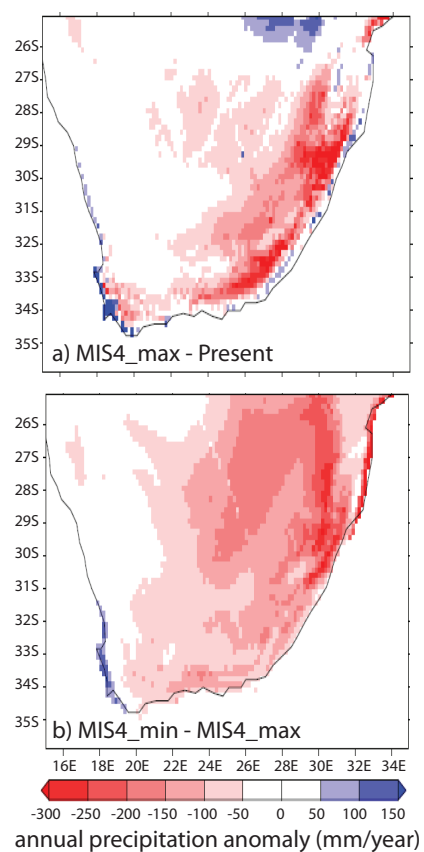


Fig. 8. Annual precipitation (mm/year) simulated by IPSL_CM5A and downscaled to 0.16° for a) MIS4_max - present, b) MIS4_min - MIS4_max.

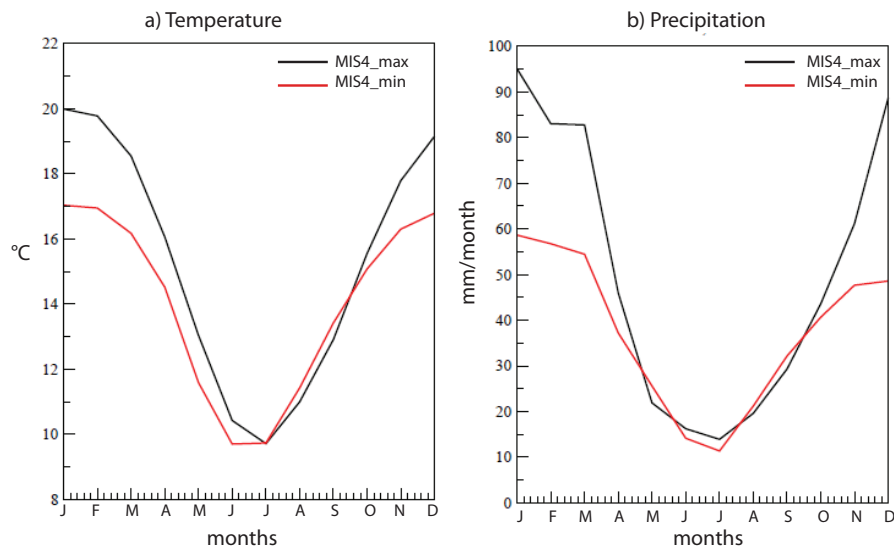


Fig. 9. Annual cycle of a) mean monthly temperatures (°C) and b) mean monthly precipitation (mm/month) over the East of southern Africa (summer rainfall area, latitude=37/25°S, longitude=22/35° simulated in MIS4_max (black) and MIS4_min (red) (IPSL_CM5A simulations, downscaled to 0.16°).

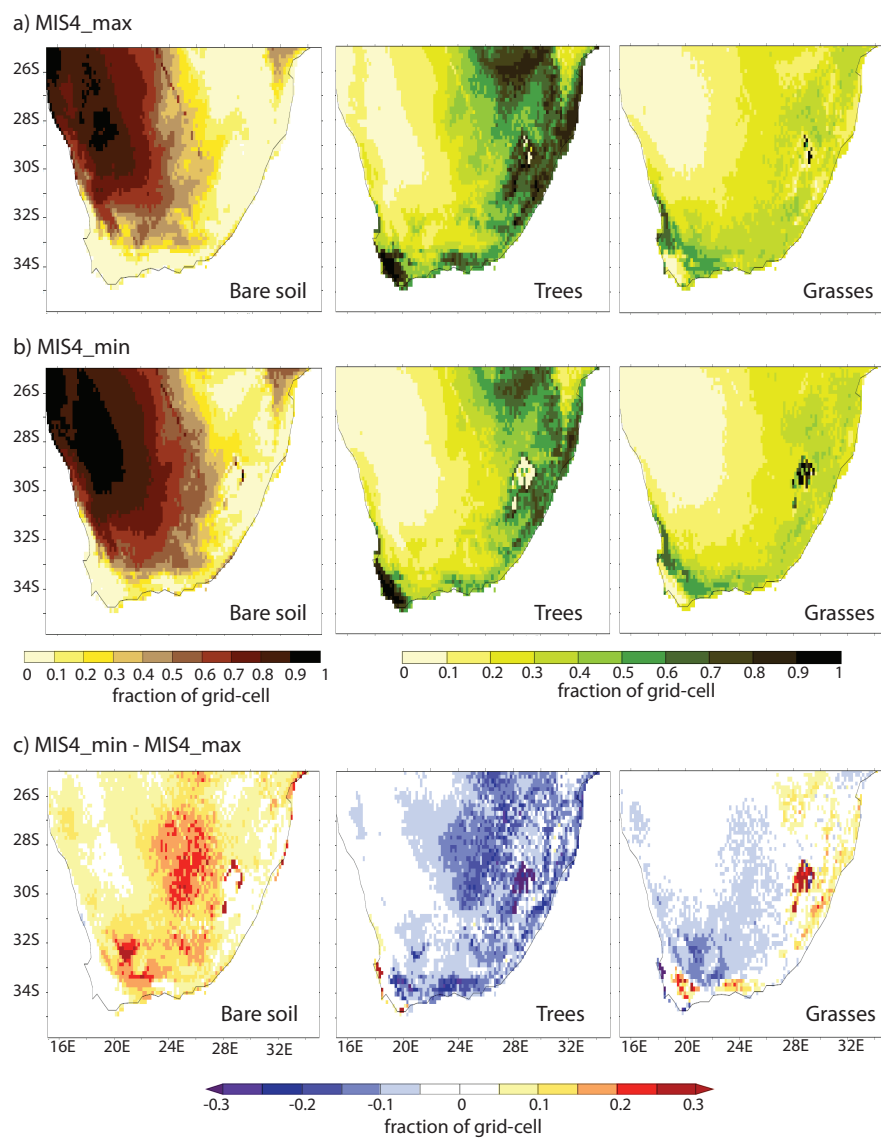


Fig. 10. Vegetation cover (fraction of grid-cell) simulated with LPJ-LMfire forced off-line. a) MIS4_max, b) MIS4_min, c) MIS4_min - MIS4_max.

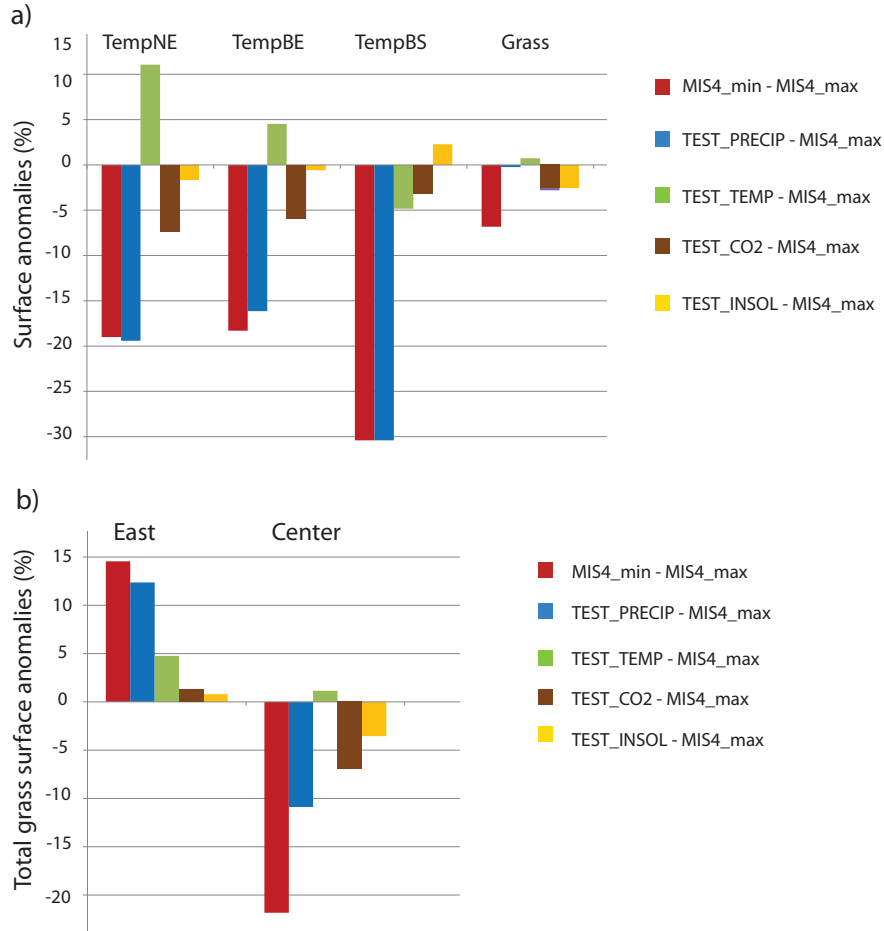


Fig. 11. a) Percentage of changes in a) the total surface occupied by temperate needleleave trees (TempNE), temperate broadleaved evergreen trees (TempBE), temperate broadleaved summergreen trees (TempBS) and grasses; b) the total surface occupied by grasses in the East (lat=34/25°S, lon=27/34°E) and in the Center (lat = 33/25°S, lon = 19/27°E) of southern Africa, in MIS4_min, TEST.PRECIP, TEST.TEMP, TEST.CO2 and TEST.INSOL compared to MIS4_max).

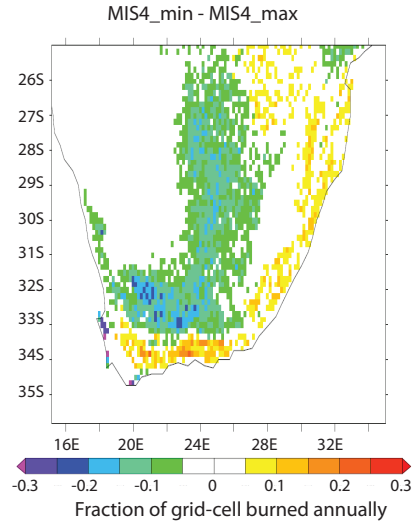


Fig. 12. Difference (MIS4_min - MIS4_max) in the percentages of a grid-cell burned during a year when precession decreases.

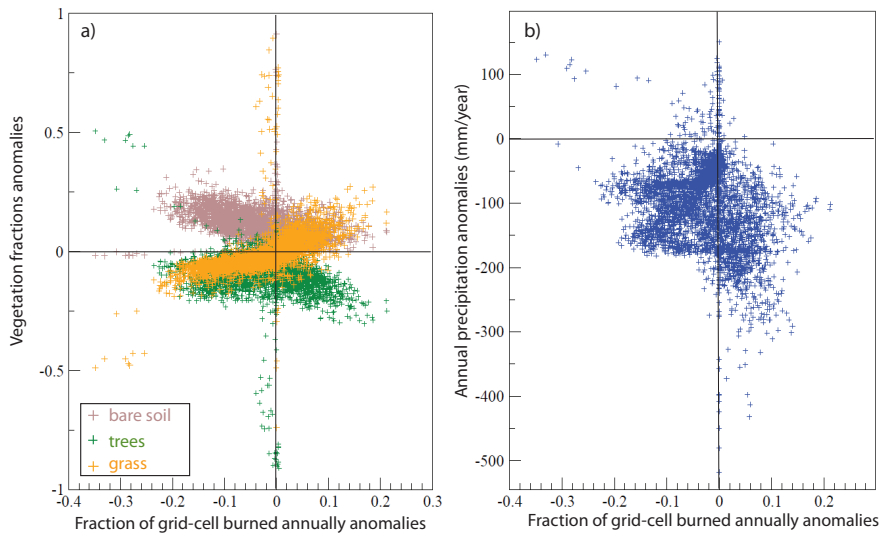


Fig. 13. a) Anomalies in the fraction of grid-cell occupied by bare soil (brown), trees (green), grasses (yellow) vs anomalies in the percentage of grid-cell burned annually (MIS4_min - MIS4_max). b) Total annual precipitation anomalies (mm/year) vs anomalies in the percentage of grid-cell burned annually (MIS4_min - MIS4_max).